research communications

Crystal structure, DFT calculation, Hirshfeld surface analysis and energy framework study of 6-bromo-2-(4-bromophenyl)imidazo[1,2-a]pyridine

Hussien Ahmed Khamees,[a] Kumara Chaluvaiah,[b] Nasseem Ahmed El-khatatneh,[a] Ananda Swamynayaka,[a] Kwong Huey Chong,[c] Jagadeesh Prasad Dasappa[b] and Mahendra Madegowda[a]*

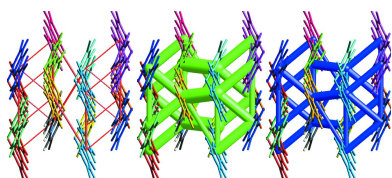[a]Department of Studies in Physics, Manasagangotri, University of Mysore, Mysuru 570 006, Karnataka, India, [b]Department of Chemistry, Mangalore University, Mangalagangothri, Mangaluru 574 199, Karnataka, India, and [c]Department of Chemistry, Faculty of Science, Universiti Putra Malaysia 43400, UPM Serdang, Selangor Darul Ehsan, Malaysia. *Correspondence e-mail: mahendra@physics.uni-mysore.ac.in

The title imidazo[1,2-a] pyridine derivative, $C_{13}H_8Br_2N_2$, was synthesized via a single-step reaction method. The title molecule is planar, showing a dihedral angle of 0.62 (17)° between the phenyl and the imidazo[1,2-a] pyridine rings. An intramolecular C—H···N hydrogen bond with an S(5) ring motif is present. In the crystal, a short H···H contact links adjacent molecules into inversion-related dimers. The dimers are linked in turn by weak C—H···π and slipped π–π stacking interactions, forming layers parallel to (110). The layers are connected into a three-dimensional network by short Br···H contacts. Two-dimensional fingerprint plots and three-dimensional Hirshfeld surface analysis of the intermolecular contacts reveal that the most important contributions for the crystal packing are from H···Br/Br···H (26.1%), H···H (21.7%), H···C/C···H (21.3%) and C···C (6.5%) interactions. Energy framework calculations suggest that the contacts formed between molecules are largely dispersive in nature. Analysis of HOMO–LUMO energies from a DFT calculation reveals the pure π character of the aromatic rings with the highest electron density on the phenyl ring, and σ character of the electron density on the Br atoms. The HOMO–LUMO gap was found to be 4.343 eV.
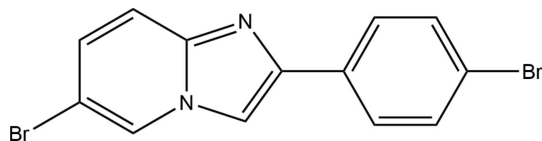
1. Chemical context

Five-membered heterocyclic compounds comprising a nitrogen atom and at least one other non-carbon atom (i.e. nitrogen, sulfur, or oxygen) as part of the ring are known as azoles. To date, numerous azoles have found a wide range of applications in various fields, including agriculture (Berger et al., 2017), and because of their biological activities (Pozharskii et al., 2011; Kumbar et al., 2018). Among the various classes of azoles, the imidazole moiety with two nitrogen atoms is extremely common in nature and forms the core of many biomolecules (Chopra & Sahu, 2019) and synthetic drugs (Pozharskii et al., 2011). Furthermore, pyridine and its derivatives are present in many important compounds, including pharmaceuticals, vitamins (Al-Ghorbani et al., 2016) and drugs, acting as antimicrobial, antiviral, antioxidants, antidiabetic, anti-malarial, anti-inflammatory or antiamoebic agents, as well as psychopharmacological antagonists (Altaf et al., 2015). Hence, the combination of pyridine and imidazole derivatives has been proven to result in highly active agents in

diverse biological fields that include anticancer (Kamal *et al.*, 2014; Mantu *et al.*, 2016), anti-HIV (Bode *et al.*, 2011), antibacterial (Rival *et al.*, 1992) and anti-inflammatory (Rupert *et al.*, 2003) properties. In addition, such a combination showed significant activity against the human *cytomegalo* virus and the *varicella-zoster* virus (Gueiffier *et al.*, 1998; Mavel *et al.*, 2002).

In this context, we synthesized a new imidazo[1,2-*a*] pyridine derivative, $C_{13}H_8Br_2N_2$, and report herein its molecular and crystal structure, as well as the quantification of supramolecular interactions by Hirshfeld surface analysis. This study is supplemented by DFT calculations and a comparison of structural details with related compounds.

2. Structural commentary

The molecular structure of the title compound is depicted in Fig. 1. The molecular system is planar, showing a dihedral angle of 0.62 (17)° between the phenyl ring (C1–C6) and the imidazo[1,2-*a*] pyridine ring system (C7–C13,N1,N2). The torsion angles about the terminal bromine atoms, Br1 and Br2, are 177.3 (3)° (Br1—C1—C6—C5) and −178.9 (4)° (Br2—C11—C12—C13), respectively. The planar arrangement between the two rings enables an intramolecular C—H···N interaction (Fig. 1, Table 1) forming an $S(5)$ ring motif (Tan & Tiekink, 2019). The Br1—C1 and Br2—C11 bond lengths are 1.886 (4) Å and 1.880 (4) Å, respectively, in good agreement with structures comprising bromophenyl moieties (Zhang & Hu, 2005; Arif Tawfeeq *et al.*, 2019). The N1=C9 bond is slightly longer than similar bonds of reported imidazo[1,2-*a*] pyridine structures (see §7 for a listing of these structures), which may be attributed to the presence of the intramolecular bond (H5···N1). Overall, the bond lengths and angles of the phenyl ring and the imidazo[1,2-*a*]pyridine ring system are in normal ranges and compare well with those of other imidazo[1,2-*a*]pyridine derivatives (Zhang *et al.*, 2005; Dhanalakshmi *et al.*, 2018).
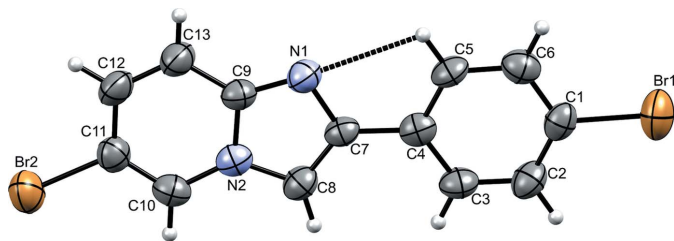
Table 1
Hydrogen-bond geometry (Å, °).

$Cg3$ is the centroid of C1–C6 ring

D—H···A	D—H	H···A	D···A	D—H···A
C5—H5···N1	0.93	2.47	2.827 (5)	103
C3—H3···$Cg3^i$	0.93	2.91	3.5670 (1)	129

Symmetry code: (i) $x, -y-\frac{3}{2}, z-\frac{1}{2}$.

3. Supramolecular features

The crystal packing is mainly based on short contacts and weak π–π interactions, similar to reported structures with the same kind of terminal bromine atoms (Arif Tawfeeq *et al.*, 2019). In the title compound, two inversion-related molecules are linked by a short H5···H5(1 − x, 2 − y, z) contact (Fig. 2). These dimers are connected to each other through C—H···π interactions (Table 1), forming sheets propagating parallel to (110). Slipped π–π stacking interactions [$Cg3$···$Cg1(−x, 1 − y, −z)$ = 3.655 (2) Å, slippage of 0.885 Å; $Cg3$···$Cg2(−x, 1 − y, −z)$ = 3.819 (2) Å, slippage of 1.473 Å], where $Cg1$, $Cg2$ and $Cg3$ are the centroids of the imidazole, pyridine and phenyl rings, respectively, are also present within these sheets (Fig. 2). Adjacent sheets are linked along [001] into a three-dimensional network through short contacts of 3.01 Å between Br1 and H12($x, \frac{3}{2} − y, \frac{1}{2} + z$), forming $S(11)$ chain motifs (Fig. 3).

Figure 1
The molecular structure of the title compound with displacement ellipsoids drawn at the 50% probability level. The intramolecular C—H···N hydrogen bond forming an $S(5)$ ring motif is shown with dashed lines.
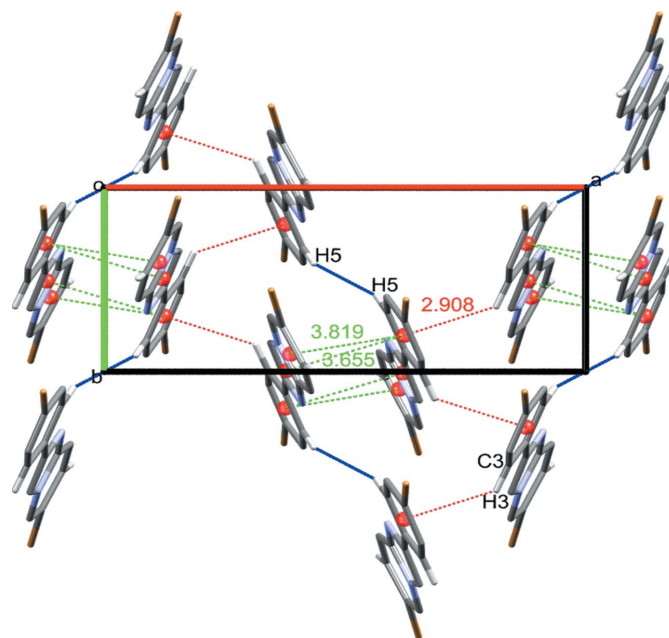

Figure 2
The crystal packing of the title compound in a view along [001], showing interactions in the sheets. H5···H5 short contacts are represented as blue dashed lines, C3—H3···$Cg3$ interactions as red dashed lines (slippage 1.676 Å) and $Cg3$···$Cg1$ and $Cg3$···$Cg2$ interactions as light-green dashed lines.
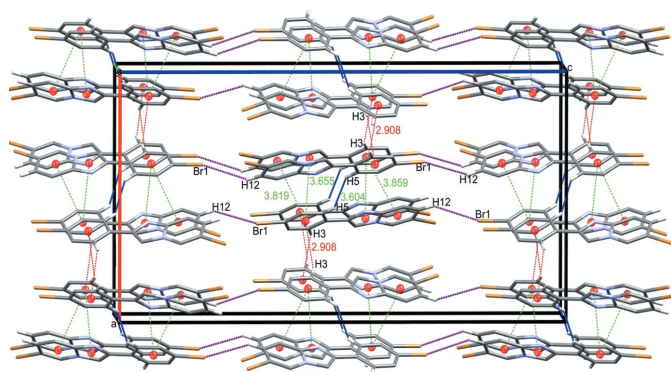
Figure 3
The three-dimensional supramolecular network of the title compound viewed approximately along [010].

4. DFT study and FMOs

Density functional theory (DFT) calculations were carried out by using the B3LYP basis set (Becke, 1993) at the highest basis set level of 6-311 ++G(d,p) in the *GAUSSIAN09* program (Frisch *et al.*, 2009). The DFT-optimized structure of the title compound is generally found to be in good agreement with the experimental data for all bond lengths and angles.

Frontier molecular orbitals (FMOs) are useful to specify the distribution of electronic densities and other quantum chemical parameters including hardness (η), softness (ζ), chemical potential (μ), electrophilicity (ψ) and electronegativity (χ) by foreseeing the highest occupied molecular orbitals (HOMO) and the lowest-unoccupied molecular
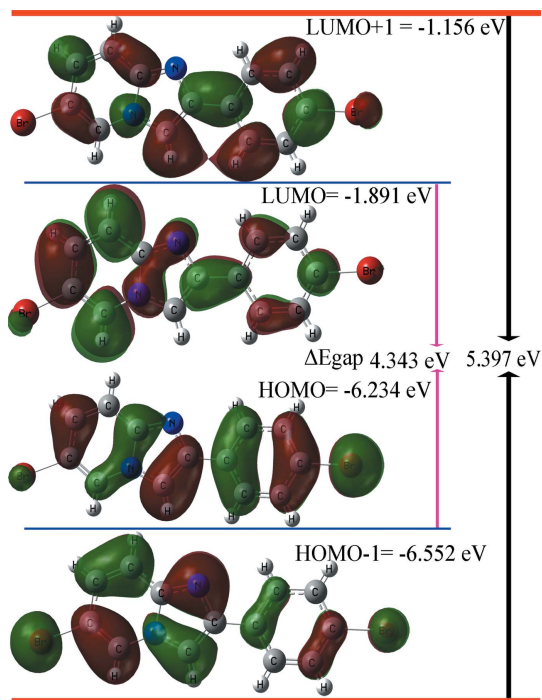

Figure 4
Electron distribution and molecular orbital energies of HOMO-1, HOMO, LUMO and LUMO+1 of the title compound.

Table 2
HUMO–LUMO energies and values of quantum chemical parameters (eV).

Property	Symbol and formula	Value
HOMO energy	E_H (eV)	−6.234
LUMO energy	E_L (eV)	−1.891
HOMO-1 energy	E_{H-1} (eV)	−6.552
LUMO+1 energy	E_{L+1} (eV)	−1.156
Energy gap 1	$E_{g1} = (E_H - E_L)$ (eV)	4.343
Energy gap 2	$E_{g2} = (E_{H-1} - E_{L+1})$ (eV)	5.397
Global hardness	$\eta = (E_L - E_H)/2$	2.172
Softness	$\zeta = 1/2\eta$	0.230
Chemical potential	$\mu = (E_L + E_H)/2$	4.062
Electrophilicity	$\psi = \mu^2/2\eta$	3.799
Electronegativity	$\chi = -\mu$	−4.062

orbitals (LUMO), as well as the energy gap ($E_g = E_H - E_L$) (Khamees *et al.*, 2018). The results of these calculations are compiled in Table 2, and orbital energy plots of (E_H, E_{H-1}) and (E_L, E_{L+1}) are depicted in Fig. 4. The HOMO (ground state) manifests the highest π characterization for phenyl ring (C1–C6) that displays bifurcated π–π stacking interactions as well as C—H$\cdots\pi$ interactions in the supramolecular network, as discussed in Section 3. Pronounced σ character of the electron density is located on the two Br atoms, with the higher amount located on Br1. The other FMOs orbitals, *i.e.* HOMO-1, LUMO and LUMO+1, exhibit a mix of π and σ character on the rings with variations of the electron density distribution (Fig. 4). The HOMO–LUMO gap is 4.343 eV for the title compound.

5. Hirshfeld surface analysis

The nature of intermolecular interactions in the title compound has been computed by *CrystalExplorer17.5* (Turner *et al.*, 2017), using Hirshfeld surface analysis (Spackman & Jayatilaka, 2009) and two-dimensional fingerprint plots (McKinnon *et al.*, 2007). The d_{norm} plot was estimated *via* calculations of the external (d_e) and internal (d_i) distances to the nearest nucleus and built over the volume of 363.34 Å^3 and an area of 339.81 Å^2, with scaled colour of −0.1544 (red) a.u. to 1.0479 (blue) a.u. (Fig. 5a). The plots of shape-index and curvedness were generated in the range of −4.0 to 4.0 a.u. and
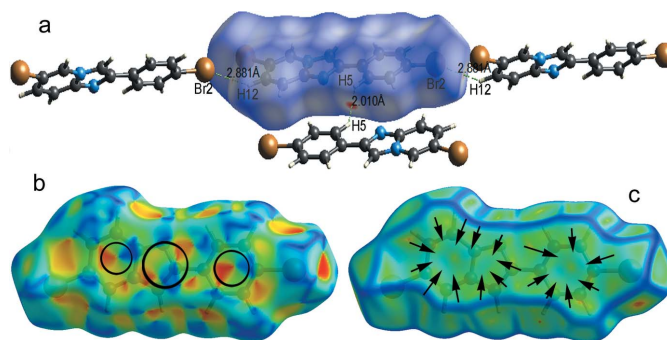

Figure 5
(a) Hirshfeld surface mapped over d_{norm} showing short contacts as green dashed lines, (b) shape-index map and (c) curvedness map showing regions of π–π interactions.

−1.00 to 1.00 a.u., respectively, (Fig. 5*b,c*). The medium dark and side pale-red spots on the Hirshfeld surface (Fig. 5*a*) symbolize the H5···H5 and Br1···H12 short contacts, respectively. The two-dimensional fingerprint plot for all contacts is depicted in Fig. 6*a*. The H···Br/Br···H contacts make the largest contribution (26.1%) to the Hirshfeld surface (Fig. 6*b*). These contacts also make a significant contribution to the crystal packing as the distance between the atoms involved is slightly less than their van der Waals radii ($d_i + d_e$ $\simeq$ 3.01 Å). The interatomic contacts of H···H interactions generated 22.7% of the Hirshfeld surface (Fig. 6*c*), showing a short spike at diagonal axes $d_i + d_e \simeq 2.24$ Å < 2.4 Å, denoting H···H short contacts with another significant effect on the molecular packing. The two symmetrical broad wings in Fig. 6*d* belong to H···C/C···H contacts that represent 21.3% of total surface and indicate the presence of C—H···π interactions in the crystal packing, where $d_i + d_e \simeq 2.77$ Å < 2.90 Å. The proportion of H···N/N···H contacts is 7.9% of the Hirshfeld surface (Fig. 6*e*) and they appear as two close wings pointing at
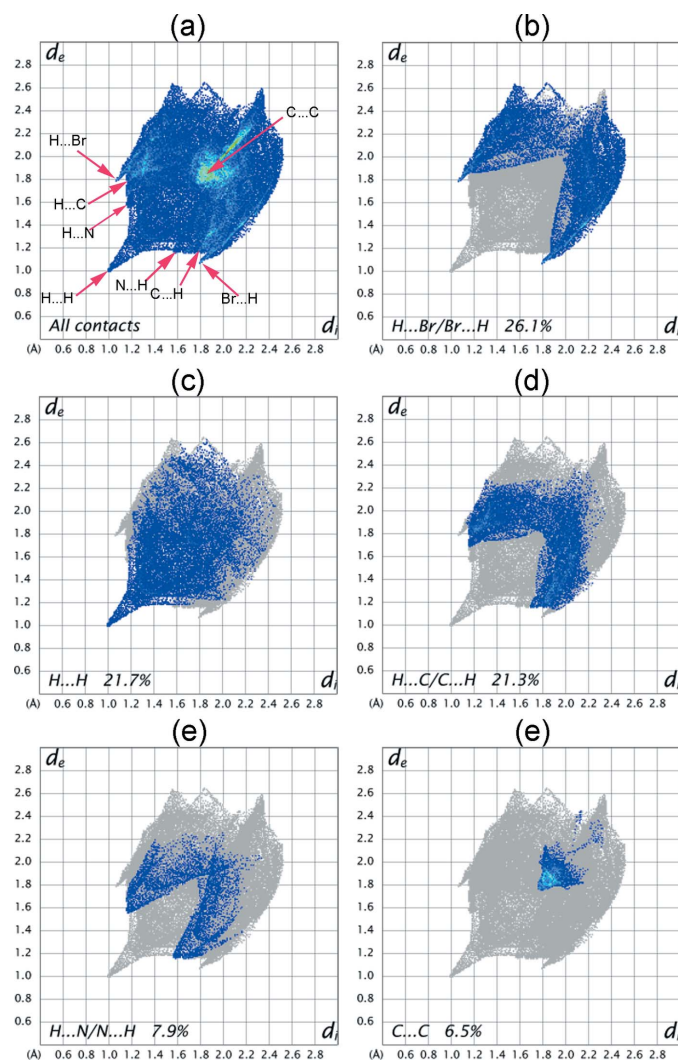
a distance greater than the van der Waals radii of N and H atoms ($d_i + d_e$ > 2.75Å), with no significant contribution towards the crystal packing of the title molecule. The small contribution of the C···C contacts (6.5%) to the Hirshfeld surface appears as an intense triangle (Fig. 6*f*) at $d_i + d_e \simeq$ 3.6 Å, indicating π–π stacking interactions in the crystal packing. This type of stacking interaction appears as a flat region on the curvedness (Fig. 5*c*) and also on the shape-index as red and blue triangles on the rings (Fig. 5*b*), in particular on the phenyl ring (C1–C6). The contributions from other contacts have negligible effects on the packing.

6. Energy framework

Quantification of energy framework energies is considered a powerful method for understanding the topology of the overall interactions of molecules in the crystal. This method allowed us to calculate and compare different energy components, *i.e.* repulsion (E_rep), electric (E_ele), dispersion (E_dis), polarization (E_pol) and total (E_tot) energy based on the anisotropy of the topology of pairwise intermolecular interaction energies. *CrystalExplorer17.5* (Turner *et al.*, 2017) was used to calculate the energy framework of the title compound by generating new wave functions using the DFT method under 3-21G basis set with exchange and potential functions (B3LYP) for a molecular cluster environment for a 1×1×1 unit cell. The thickness of the cylinder radius indicates the grade of interactions and is directly related to the energy magnitude and offers information about the stabilization of the crystal packing. In order to avoid the crowdedness of less significant interaction energies, we set the cylindrical radii with a cut-off value of 5 kJ mol^{-1} and a scale factor of 50 to all

Figure 6
Two-dimensional fingerprint plots of the title molecule with their relative contributions to the Hirshfeld surface.

N	Symop	R	E_ele	E_pol	E_dis	E_rep	E_tot
2	-x+1/2, y+1/2, z	4.85	-5.7078	-2.664	-45.7275	15.3882	-38.7111
1	x+1/2, -y+1/2, -z	7.8	0.5285	-0.074	-2.4388	0	-1.9843
2	x, -y+1/2, z+1/2	14.15	-0.5285	-0.222	-6.6196	3.0282	-4.3419
1	-x, -y, -z	3.95	-2.3254	-2.368	-67.7638	21.3828	-51.0744
1	-x, y+1/2, -z+1/2	13.22	-0.2114	-0.074	-3.7453	0.4326	-3.5981
1	x, y, z	6.05	-10.6757	-1.628	-25.6074	8.8992	-29.0119
2	-x+1/2, -y, z+1/2	14.28	-0.5285	-0.074	-3.6582	1.2978	-2.9629
1	-x, -y, -z	7.10	-9.9358	-0.072	-24.9977	11.8038	-25.2017
	Total		-29.38	-9.176	-180.558	62.232	-156.886

Figure 7
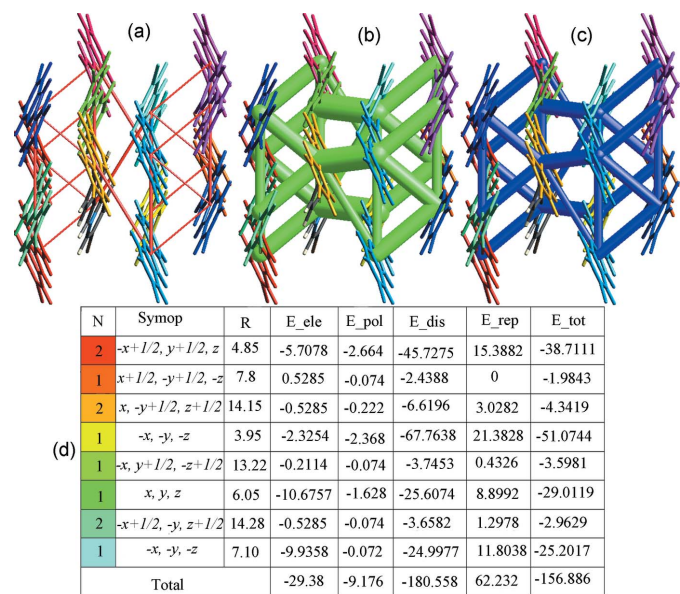Energy framework of the title molecules viewed along [001], showing: (*a*) electrostatic, (*b*) dispersion, (*c*) total energy force diagrams and (*d*) the details of interaction with colour-coded, symmetry operation (Symop) and distances between molecular centroids (*R*) in Å.

Table 3
Comparison of structural details in related imidazo[1,2-*a*]pyridinyl derivatives containing phenyl rings.

Dihedral angle 1 is the angle between the mean planes of imidazo[1,2-*a*]pyridinyl and phenyl rings. Two sets of dihedral angles 1 are stated for compounds HURZOL, MONREO, OMIDEV, RUJNEQ, TUZYEU, ZUSSAJ and VEGKAU because there are two molecules in their asymmetric units.

Compound	R_1	R_2	Dihedral angle 1
3-(Substituted)imidazo[1,2-*a*]pyridinyl			
AHOMIV (Liu *et al.*, 2015)	6-iodo-3-(methylsulfanyl)-imidazo[1,2-*a*]pyridinyl	phenyl	27.0
BEGTUE (Nair *et al.*, 2012)	ethyl (imidazo[1,2-*a*]pyridin-3-yl)acetate	phenyl	38.6
DABTEI (Koudad *et al.*, 2015)	6-nitroimidazo[1,2-*a*]pyridinyl-3-carbaldehyde	4-methoxyphenyl	34.0
DIDZUO (Dey *et al.*, 2018)	3-chloro-7-methyl-imidazo[1,2-*a*]pyridinyl	phenyl	28.0
ECEGEA (Ma *et al.*, 2011)	ethyl 8-methyl-imidazo[1,2-*a*]pyridinyl-3-carboxylate	phenyl	44.2
HUPWIZ01 (Vega *et al.*, 2011)	*N,N*-dimethyl-2-(6-methyl-imidazo[1,2-*a*]pyridin-3-yl)aceta-mide	4-methylphenyl	24.6
HURZOL (Yang *et al.*, 2015)	6-methylimidazo[1,2-*a*]pyridin-3-yl thiocyanate	3-chlorophenyl	33.8, 27.7
KABMIM (Yang *et al.*, 2016)	6-methyl-3-nitrosoimidazo[1,2-*a*]pyridinyl	3-chlorophenyl	6.8
MIXZOJ (Anaflous *et al.*, 2008*a*)	*N*-(imidazo[1,2-*a*]pyridin-3-yl)acetamide	phenyl	9.0
MIXZUP (Anaflous *et al.*, 2008*b*)	imidazo[1,2-*a*]pyridinyl-3-carbaldehyde	phenyl	28.6
MONREO (Velázquez-Ponce *et al.*, 2013)	3-nitrosoimidazo[1,2-*a*]pyridinyl	phenyl	17.4, 4.9
NOGRIM (Marandi *et al.*, 2014)	3-(*t*-butylamino)-imidazo[1,2-*a*]pyridinyl-8-carboxylic acid	3-nitrophenyl	16.8
OMIDEV (Samanta *et al.*, 2016)	3-iodo-8-methyl-imidazo[1,2-*a*]pyridinyl	phenyl	36.1, 34.4
QUQSEC (Ravi *et al.*, 2016)	6-methyl-3-(methylsulfanyl)imidazo[1,2-*a*]pyridinyl	4-chlorophenyl	38.1
RELQUW (Yan *et al.*, 2012)	8-methyl-3-nitroimidazo[1,2-*a*]pyridinyl	phenyl	47.5
RUJNEQ (Li *et al.*, 2009)	imidazo[1,2-*a*]pyridinyl-3-carbaldehyde	4-chlorophenyl	34.6, 33.5
TUZYEU (Zhang *et al.*, 2016)	6-fluoro-3-nitro-imidazo[1,2-*a*]pyridinyl	phenyl	43.8, 37.9
UTITEX (Chunavala *et al.*, 2011)	ethyl 7-methylimidazo[1,2-*a*]pyridinyl-3-carboxylate	phenyl	39.6
YEDHIY (Georges *et al.*, 1993)	6-chloro-*N,N*-dipropylimidazo[1,2-*a*] pyridinyl-3-acetamide	4-chlorophenyl	15.2
ZUSSAJ (Xiao *et al.*, 2015)	3-chloro-imidazo[1,2-*a*]pyridinyl	4-methylphenyl	12.0, 0.3
Non-3-(substituted)imidazo[1,2-*a*]pyridinyl			
BISDUF (Kutniewska *et al.*, 2018)	imidazo[1,2-*a*]pyridinyl	2-hydroxy-5-methoxyphenyl	6.0
BISFAN (Kutniewska *et al.*, 2018)	imidazo[1,2-*a*]pyridinyl	2-hydroxy-4-bromophenyl	4.2
CAJTIQ (Aslanov *et al.*, 1983)	6-nitro-imidazo[1,2-*a*]pyridinyl	phenyl	3.3
FEMQOF (Kurteva *et al.* 2012)	imidazo[1,2-*a*]pyridinyl	4-methoxyphenyl	12.5
JEBZEY (Zhu *et al.*, 2017)	imidazo[1,2-*a*]pyridinyl	isophthalonitrile	46.4
MIQSUD (Jin *et al.*, 2019)	2-(imidazo[1,2-*a*]pyridin-5-yl)propan-2-ol	phenyl	2.7
NAGGEH (Tafeenko *et al.*, 1996)	imidazo[1,2-*a*]pyridinyl	phenyl	4.4
NONFOM (Mutai *et al.*, 2008)	imidazo[1,2-*a*]pyridinyl	2-hydroxyphenyl	6.7
NUBVUD (Seferoğlu *et al.*, 2015)	7-methylimidazo[1,2-*a*]pyridinyl	4-methoxyphenyl	0.7
NUBWAK (Seferoğlu *et al.*, 2015)	7-methyl-imidazo[1,2-*a*]pyridinyl	phenyl	5.3
QODZUG (Mutai *et al.*, 2014)	imidazo[1,2-*a*]pyridinyl-6-carbonitrile	2-hydroxyphenyl	2.8
TIDVIN (Donohoe *et al.*, 2012)	6-bromo-imidazo[1,2-*a*]pyridinyl	phenyl	2.4
VEGKAU (Duan *et al.*, 2006)	imidazo[1,2-*a*]pyridinyl	3-bromo-4-methoxyphenyl	12.2, 2.7
WUHKER (Aydıner *et al.*, 2015)	7-methylimidazo[1,2-*a*]pyridinyl	4-chlorophenyl	9.1
ZUNVOV (Stasyuk *et al.*, 2016)	imidazo[1,2-*a*]pyridinyl	2-hydroxy-4-florophenyl	3.2
ZUPCOE (Stasyuk *et al.*, 2016)	imidazo[1,2-*a*]pyridinyl	2-hydroxy-4-methoxyphenyl	5.8

energy components. The benchmarked energies were scaled according to Mackenzie *et al.* (2017) while *E*_rep, *E*_ele, *E*_dis and *E*_pol were scaled as 0.618, 1.057, 0.740, 0.871, respectively (Edwards *et al.*, 2017). The results of the calculations revealed that dispersion interactions exhibit approximately chair-shaped energy topologies through the rings, having a maximum energy value of −180.558 kJ mol⁻¹ (Fig. 7). The other energy components have values of 62.232 kJ mol⁻¹, −29.38 kJ mol⁻¹ and −9.176 kJ mol⁻¹ for repulsion, electrostatic and polarization energies, respectively. The small value of electrostatic energy is attributed to the absence of classical hydrogen bonds. The total interaction energy that resulted from all four main components is −156.886 kJ mol⁻¹ (Fig. 7*d*).

7. Database survey

36 structures containing the 2-phenylimidazo[1,2-*a*]pyridine moiety with different substituents were found in a search of the Cambridge Structural Database (CSD, version 5.40, last update May 2019; Groom *et al.*, 2016). The different substit-uents R_1 (on the imidazo[1,2-*a*]pyridinyl ring) and R_2 (on the phenyl ring) together with the dihedral angles between the mean planes of the corresponding imidazo[1,2-*a*]pyridinyl and phenyl rings (dihedral angle 1) are compiled in Table 3. By comparing the substitution positions, the structures can be divided into '3-(substituted)imidazo[1,2-*a*]pyridinyl' compounds and 'non-3-(substituted)imidazo[1,2-*a*]pyridinyl' compounds. In general, the 3-(substituted)imidazo[1,2-*a*]-pyridinyl compounds have a greater dihedral angle 1 values (12.0–47.5°). This may arise from steric repulsion between the 3-(substituted) group and the phenyl ring. However, there are four outliers (KABMIM, MIXZOJ, MONREO and ZUSSAJ) whose dihedral angle 1 values are lower than 10°. Most of the non-3-(substituted)imidazo[1,2-*a*]pyridinyl compounds have dihedral angle 1 values between 0.7 and 12.5°, which indicates that the imidazo[1,2-*a*]pyridinyl rings are close to coplanar to their attached phenyl rings. Here, the outlier is JEBZEY where the imidazo[1,2-*a*]pyridinyl ring is attached to a di-*ortho*-substituted isophthalonitrile ring. The dihedral angle 1 is 46.4° in this structure.

Table 4
Experimental details.

Crystal data	
Chemical formula	$C_{13}H_8Br_2N_2$
M_r	352.03
Crystal system, space group	Orthorhombic, $Pbca$
Temperature (K)	293
a, b, c (Å)	14.1711 (4), 6.0546 (2), 27.7102 (8)
V (Å^3)	2377.54 (12)
Z	8
Radiation type	Mo $K\alpha$
μ (mm^{-1})	6.80
Crystal size (mm)	$0.15 \times 0.14 \times 0.14$
Data collection	
Diffractometer	Bruker Kappa APEXII CCD
No. of measured, independent and observed [$I > 2\sigma(I)$] reflections	41143, 3485, 1726
R_{int}	0.100
$(\sin\theta/\lambda)_{max}$ (Å^{-1})	0.704
Refinement	
$R[F^2 > 2\sigma(F^2)]$, $wR(F^2)$, S	0.047, 0.118, 1.00
No. of reflections	3485
No. of parameters	154
H-atom treatment	H-atom parameters constrained
$\Delta\rho_{max}$, $\Delta\rho_{min}$ (e Å^{-3})	0.88, −0.49

Computer programs: *APEX2* and *SAINT* (Bruker, 2016), *SHELXT* (Sheldrick, 2015*a*), *SHELXL* (Sheldrick, 2015*b*), *Mercury* (Macrae *et al.*, 2008), *PLATON* (Spek, 2009) and *publCIF* (Westrip, 2010).

8. Synthesis and crystallization

5-Bromopyridin-2-amine (1.211 g, 0.007 mol) and phenacyl bromide (0.007 mol) were refluxed for 14 h in 50 ml of absolute ethanol. The progress of the reaction was monitored by thin layer chromatography using Merck alumina backed silica gel 60 F254. After completion of the reaction, the resulting product was poured into crushed ice to obtain a fine grained solid product that was filtered off, separated and dried. The crude product was then recrystallized from hot ethanol with a yield of ~70%. The melting point of 345 K was determined in an open capillary and is uncorrected. IR (KBr, cm^{-1}): 3080 (Ar C—H stretch), 2918 (aliphatic C—H stretch, 4-bromophenyl moiety), 1587 (C=N stretch), 1332 (C—N), 792 and 595 (C—Br). ^{1}H NMR (400 MHz, DMSO, δ ppm): 7.37 (*d*, 1H, 5-bromopyridine moiety), 7.55 (*d*, 2H, 4-bromophenyl moiety), 7.56 (*d*, 1H, 5-bromopyridine moiety), 7.78 (*d*, 2H, 4-bromophenyl moiety), 8.37 (*s*, 1H, imidazole ring), 8.87 (*s*, 1H, 5-bromopyridine moiety). ^{13}C NMR (400 MHz, δ ppm): 145.13 (imidazopyridine carbon atom), 110.24, 119.82, 125.12 and 132.14 (four carbon atoms of 5-bromopyridine moiety), 123.12, 128.30, 132.11, and 132.32 (six carbon atoms of 4-bromophenyl moiety), 113.13 and 130.10 (two carbon atoms of imidazole ring). LC–Mass *m/z* 350 [M+], 352 [*M*+2], 354 [*M*+4]. Analysis calculated for $C_{13}H_8Br_2N_2$ (350): C, 44.36; H, 2.29; N, 7.96. Found: C, 44.31; H, 2.23; N, 7.92%.

9. Refinement

Crystal data, data collection and structure refinement details are summarized in Table 4. Hydrogen atoms were placed in calculated positions (C—H = 0.93 Å) and were included in the refinement in the riding-model approximation, with U_{iso}(H) set to $1.2U_{eq}$(C). The reflection (002) was affected by the beam-stop and was removed from the refinement

References

Al-Ghorbani, M., Thirusangu, P., Gurupadaswamy, H. D., Girish, V., Shamanth Neralagundi, H. G., Prabhakar, B. T. & Khanum, S. A. (2016). *Bioorg. Chem.* **65**, 73–81.

Altaf, A. A., Shahzad, A., Gul, Z., Rasool, N., Badshah, A., Lal, B. & Khan, E. (2015). *J. Drug Des. Med. Chem.* **1**, 1–11.

Anaflous, A., Albay, H., Benchat, N., El Bali, B., Dušek, M. & Fejfarová, K. (2008*a*). *Acta Cryst.* E**64**, o926.

Anaflous, A., Albay, H., Benchat, N., El Bali, B., Dušek, M. & Fejfarová, K. (2008*b*). *Acta Cryst.* E**64**, o927.

Arif Tawfeeq, N., Kwong, H. C., Mohamed Tahir, M. I. & Ravoof, T. B. S. A. (2019). *Acta Cryst.* E**75**, 774–779.

Aslanov, L. A., Tafeenko, V. A., Paseshnichenko, K. A., Bundel, Y. G., Gromov, S. P. & Gerasimov, B. G. (1983). *Zh. Strukt. Khim.* **24**, 115–123.

Aydıner, B., Yalçın, E., Ihmels, H., Arslan, L., Açık, L. & Seferoğlu, Z. (2015). *J. Photochem. Photobiol. Chem.* **310**, 113–121.

Becke, A. D. (1993). *J. Chem. Phys.* **98**, 5648–5652.

Berger, S., El Chazli, Y., Babu, A. F. & Coste, A. T. (2017). *Front. Microbiol.* **8**, 1–6.

Bode, M. L., Gravestock, D., Moleele, S. S., van der Westhuyzen, C. W., Pelly, S. C., Steenkamp, P. A., Hoppe, H. C., Khan, T. & Nkabinde, L. A. (2011). *Bioorg. Med. Chem.* **19**, 4227–4237.

Bruker (2016). *APEX2* and *SAINT*. Bruker AXS Inc., Madison, Wisconsin, USA.

Chopra, P. N. & Sahu, J. K. (2019). *Curr. Drug Discov. Technol.* **1**, 1570–1638.

Chunavala, K. C., Joshi, G., Suresh, E. & Adimurthy, S. (2011). *Synthesis*, **2011**, 635–641.

Dey, A., Singsardar, M., Sarkar, R. & Hajra, A. (2018). *ACS Omega* **3**, 3513–3521.

Dhanalakshmi, G., Ramanjaneyulu, M., Thennarasu, S. & Aravindhan, S. (2018). *Acta Cryst.* E**74**, 1913–1918.

Donohoe, T. J., Kabeshov, M. A., Rathi, A. H. & Smith, I. E. D. (2012). *Org. Biomol. Chem.* **10**, 1093–1101.

Duan, G.-Y., Tu, C.-B., Sun, Y.-W., Zhang, D.-T. & Wang, J.-W. (2006). *Acta Cryst.* E**62**, o1141–o1142.

Edwards, A. J., Mackenzie, C. F., Spackman, P. R., Jayatilaka, D. & Spackman, M. A. (2017). *Faraday Discuss.* **203**, 93–112.

Frisch, M. J., Trucks, G. W., Schlegel, H. B., Scuseria, G. E., Robb, M. A., Cheeseman, J. R., *et al.* (2009). *GAUSSIAN09*. Gaussian Inc., Wallingford, CT, USA.

Georges, G. J., Vercauteren, D. P., Evrard, G. H., Durant, F. V., George, P. G. & Wick, A. E. (1993). *Eur. J. Med. Chem.* **28**, 323–335.

Groom, C. R., Bruno, I. J., Lightfoot, M. P. & Ward, S. C. (2016). *Acta Cryst.* B**72**, 171–179.

Gueiffier, A., Mavel, S., Lhassani, M., Elhakmaoui, A., Snoeck, R., Andrei, G., Chavignon, O., Teulade, J. C., Witvrouw, M., Balzarini, J., De Clercq, E. & Chapat, J. (1998). *J. Med. Chem.* **41**, 5108–5112.

Jin, S., Xie, B., Lin, S., Min, C., Deng, R. & Yan, Z. (2019). *Org. Lett.* **21**, 3436–3440.

Kamal, A., Reddy, V. S., Santosh, K., Bharath Kumar, G., Shaik, A. B., Mahesh, R., Chourasiya, S. S., Sayeed, I. B. & Kotamraju, S. (2014). *Med. Chem. Commun.* **5**, 1718–1723.

research communications

Khamees, H. A., Jyothi, M., Khanum, S. A. & Madegowda, M. (2018). *J. Mol. Struct.* **1161**, 199–217.

Koudad, M., Elaatiaoui, A., Benchat, N., Saadi, M. & El Ammari, L. (2015). *Acta Cryst.* E**71**, o979–o980.

Kumbar, M. N., Kamble, R. R., Dasappa, J. P., Bayannavar, P. K., Khamees, H. A., Mahendra, M., Joshi, S. D., Dodamani, S., Rasal, V. P. & Jalalpure, S. (2018). *J. Mol. Struct.* **1160**, 63–72.

Kurteva, V. B., Lubenov, L. A., Nedeltcheva, D. V., Nikolova, R. P. & Shivachev, B. L. (2012). *Arkivoc*, **13**, 282–294.

Kutniewska, S. E., Jarzembska, K. N., Kamiński, R., Stasyuk, A. J., Gryko, D. T. & Cyrański, M. K. (2018). *Acta Cryst.* B**74**, 725–737.

Li, Y.-H., Liu, W.-Y., Gao, Y. & Wang, Y.-P. (2009). *Acta Cryst.* E**65**, o3192.

Liu, S., Xi, H., Zhang, J., Wu, X., Gao, Q. & Wu, A. (2015). *Org. Biomol. Chem.* **13**, 8807–8811.

Ma, L., Wang, X., Yu, W. & Han, B. (2011). *Chem. Commun.* **47**, 11333–11335.

Mackenzie, C. F., Spackman, P. R., Jayatilaka, D. & Spackman, M. A. (2017). *IUCrJ*, **4**, 575–587.

Macrae, C. F., Bruno, I. J., Chisholm, J. A., Edgington, P. R., McCabe, P., Pidcock, E., Rodriguez-Monge, L., Taylor, R., van de Streek, J. & Wood, P. A. (2008). *J. Appl. Cryst.* **41**, 466–470.

Mantu, D., Antoci, V., Moldoveanu, C., Zbancioc, G. & Mangalagiu, I. I. (2016). *J. Enzyme Inhib. Med. Chem.* **31**, 96–103.

Marandi, G., Saghatforoush, L., Mendoza-Meroño, R. & García-Granda, S. (2014). *Tetrahedron Lett.* **55**, 3052–3054.

Mavel, S., Renou, J. L., Galtier, C., Allouchi, H., Snoeck, R., Andrei, G., De Clercq, E., Balzarini, J. & Gueiffier, A. (2002). *Bioorg. Med. Chem.* **10**, 941–946.

McKinnon, J. J., Jayatilaka, D. & Spackman, M. A. (2007). *Chem. Commun.* pp. 3814–3816.

Mutai, T., Shono, H., Shigemitsu, Y. & Araki, K. (2014). *CrystEngComm*, **16**, 3890–3895.

Mutai, T., Tomoda, H., Ohkawa, T., Yabe, Y. & Araki, K. (2008). *Angew. Chem. Int. Ed.* **47**, 9522–9524.

Nair, D. K., Mobin, S. M. & Namboothiri, I. N. N. (2012). *Org. Lett.* **14**, 4580–4583.

Pozharskii, A. F., Soldatenkov, A. T. & Katritzky, A. R. (2011). Heterocycles in Life and Society. John Wiley & Sons.

Ravi, C., Chandra Mohan, D. & Adimurthy, S. (2016). *Org. Biomol. Chem.* **14**, 2282–2290.

Rival, Y., Grassy, G. & Michel, G. (1992). *Chem. Pharm. Bull.* **40**, 1170–1176.

Rupert, K. C., Henry, J. R., Dodd, J. H., Wadsworth, S. A., Cavender, D. E., Olini, G. C., Fahmy, B. & Siekierka, J. J. (2003). *Bioorg. Med. Chem. Lett.* **13**, 347–350.

Samanta, S., Jana, S., Mondal, S., Monir, K., Chandra, S. K. & Hajra, A. (2016). *Org. Biomol. Chem.* **14**, 5073–5078.

Seferoğlu, Z., Ihmels, H. & Şahin, E. (2015). *Dyes Pigments*, **113**, 465–473.

Sheldrick, G. M. (2015a). *Acta Cryst.* A**71**, 3–8.

Sheldrick, G. M. (2015b). *Acta Cryst.* C**71**, 3–8.

Spackman, M. A. & Jayatilaka, D. (2009). *CrystEngComm*, **11**, 19–32.

Spek, A. L. (2009). *Acta Cryst.* D**65**, 148–155.

Stasyuk, A. J., Bultinck, P., Gryko, D. T. & Cyrański, M. K. (2016). *J. Photochem. Photobiol. Chem.* **314**, 198–213.

Tafeenko, V., Paseshnichenko, K. & Schenk, H. (1996). *Z. Kristallogr.* **211**, 457–263.

Tan, S. L. & Tiekink, E. R. T. (2019). *Acta Cryst.* E**75**, 1–7.

Turner, M. J., McKinnon, J. J., Wolff, S. K., Grimwood, D. J., Spackman, P. R., Jayatilaka, D. & Spackman, M. A. (2017). *CrystalExplorer17. University of Western Australia.* http://hirshfeldsurface. net.

Vega, D. R., Baggio, R., Roca, M. & Tombari, D. (2011). *J. Pharm. Sci.* **100**, 1377–1386.

Velázquez-Ponce, M., Salgado-Zamora, H., Jiménez-Vázquez, H. A., Campos-Aldrete, M. E., Jiménez, R., Cervantes, H. & Hadda, T. B. (2013). *Chem. Cent. J.* **7**: 20.

Westrip, S. P. (2010). *J. Appl. Cryst.* **43**, 920–925.

Xiao, X., Xie, Y., Bai, S., Deng, Y., Jiang, H. & Zeng, W. (2015). *Org. Lett.* **17**, 3998–4001.

Yan, R.-L., Yan, H., Ma, C., Ren, Z.-Y., Gao, X.-A., Huang, G.-S. & Liang, Y.-M. (2012). *J. Org. Chem.* **77**, 2024–2028.

Yang, D., Yan, K., Wei, W., Li, G., Lu, S., Zhao, C., Tian, L. & Wang, H. (2015). *J. Org. Chem.* **80**, 11073–11079.

Yang, D., Yan, K., Wei, W., Liu, Y., Zhang, M., Zhao, C., Tian, L. & Wang, H. (2016). *Synthesis*, **48**, 122–130.

Zhang, M., Lu, J., Zhang, J.-N. & Zhang, Z.-H. (2016). *Catal. Commun.* **78**, 26–32.

Zhang, R. & Hu, Y. (2005). *Acta Cryst.* E**61**, o4037–o4038.

Zhu, X., Shen, X.-J., Tian, Z.-Y., Lu, S., Tian, L.-L., Liu, W.-B., Song, B. & Hao, X.-Q. (2017). *J. Org. Chem.* **82**, 6022–6031.

Crystal structure, DFT calculation, Hirshfeld surface analysis and energy framework study of 6-bromo-2-(4-bromophenyl)imidazo[1,2-*a*]pyridine

Hussien Ahmed Khamees, Kumara Chaluvaiah, Nasseem Ahmed El-khatatneh, Ananda Swamynayaka, Kwong Huey Chong, Jagadeesh Prasad Dasappa and Mahendra Madegowda

Computing details

Data collection: *APEX2* (Bruker, 2016); cell refinement: *SAINT* (Bruker, 2016); data reduction: *SAINT* (Bruker, 2016); program(s) used to solve structure: SHELXT (Sheldrick, 2015a); program(s) used to refine structure: *SHELXL* (Sheldrick, 2015b); molecular graphics: *Mercury* (Macrae *et al.*, 2008) and *PLATON* (Spek, 2009); software used to prepare material for publication: *publCIF* (Westrip, 2010).

6-Bromo-2-(4-bromophenyl)imidazo[1,2-*a*]pyridine

Crystal data

$C_{13}H_8Br_2N_2$	$D_x = 1.967$ Mg m^{-3}
$M_r = 352.03$	Mo $K\alpha$ radiation, $\lambda = 0.71073$ Å
Orthorhombic, *Pbca*	Cell parameters from 3485 reflections
$a = 14.1711$ (4) Å	$\theta = 2.1–30.1°$
$b = 6.0546$ (2) Å	$\mu = 6.80$ mm^{-1}
$c = 27.7102$ (8) Å	$T = 293$ K
$V = 2377.54$ (12) Å^3	Block, colourless
$Z = 8$	$0.15 \times 0.14 \times 0.14$ mm
$F(000) = 1360$	

Data collection

Bruker Kappa APEXII CCD diffractometer	$R_{int} = 0.100$
ω and φ scan	$\theta_{max} = 30.1°$, $\theta_{min} = 2.1°$
41143 measured reflections	$h = -19 \rightarrow 19$
3485 independent reflections	$k = -8 \rightarrow 8$
1726 reflections with $I > 2\sigma(I)$	$l = -39 \rightarrow 38$

Refinement

Refinement on F^2	Hydrogen site location: inferred from neighbouring sites
Least-squares matrix: full	H-atom parameters constrained
$R[F^2 > 2\sigma(F^2)] = 0.047$	$w = 1/[\sigma^2(F_o^2) + (0.0442P)^2 + 2.6166P]$
$wR(F^2) = 0.118$	where $P = (F_o^2 + 2F_c^2)/3$
$S = 1.00$	$(\Delta/\sigma)_{max} = 0.002$
3485 reflections	$\Delta\rho_{max} = 0.88$ e Å^{-3}
154 parameters	$\Delta\rho_{min} = -0.49$ e Å^{-3}
0 restraints	

Special details

Geometry. All esds (except the esd in the dihedral angle between two l.s. planes) are estimated using the full covariance matrix. The cell esds are taken into account individually in the estimation of esds in distances, angles and torsion angles; correlations between esds in cell parameters are only used when they are defined by crystal symmetry. An approximate (isotropic) treatment of cell esds is used for estimating esds involving l.s. planes.

Fractional atomic coordinates and isotropic or equivalent isotropic displacement parameters (Å²)

	x	y	z	$U_{iso}*/U_{eq}$
Br2	0.15325 (4)	0.05914 (9)	0.27691 (2)	0.0700 (2)
Br1	0.12673 (4)	0.88905 (10)	0.68410 (2)	0.0740 (2)
N2	0.1377 (2)	0.3517 (6)	0.40975 (12)	0.0449 (8)
N1	0.0885 (2)	0.6735 (6)	0.44091 (12)	0.0484 (9)
C7	0.1238 (3)	0.5400 (6)	0.47646 (14)	0.0401 (9)
C1	0.1234 (3)	0.7762 (8)	0.62067 (15)	0.0482 (11)
C11	0.1297 (3)	0.2554 (7)	0.32808 (15)	0.0498 (11)
C4	0.1241 (3)	0.6173 (7)	0.52687 (15)	0.0424 (9)
C12	0.0872 (3)	0.4597 (8)	0.31737 (16)	0.0571 (12)
H12	0.070603	0.493692	0.285760	0.069*
C8	0.1549 (3)	0.3438 (8)	0.45819 (15)	0.0479 (10)
H8	0.182324	0.228190	0.475266	0.058*
C3	0.1597 (3)	0.4933 (7)	0.56424 (16)	0.0495 (10)
H3	0.185335	0.355055	0.557750	0.059*
C6	0.0866 (3)	0.9064 (7)	0.58414 (16)	0.0539 (11)
H6	0.061410	1.044944	0.590752	0.065*
C13	0.0707 (3)	0.6058 (8)	0.35300 (15)	0.0561 (12)
H13	0.041977	0.740195	0.346048	0.067*
C2	0.1582 (3)	0.5687 (8)	0.61068 (16)	0.0532 (11)
H2	0.180652	0.480001	0.635558	0.064*
C5	0.0885 (3)	0.8244 (7)	0.53745 (15)	0.0479 (10)
H5	0.065063	0.911265	0.512485	0.057*
C9	0.0968 (3)	0.5559 (7)	0.40055 (15)	0.0442 (10)
C10	0.1555 (3)	0.2005 (7)	0.37352 (15)	0.0492 (11)
H10	0.184202	0.065712	0.380142	0.059*

Atomic displacement parameters (Å²)

	U^{11}	U^{22}	U^{33}	U^{12}	U^{13}	U^{23}
Br2	0.0853 (4)	0.0701 (4)	0.0545 (3)	0.0001 (3)	0.0150 (3)	−0.0104 (2)
Br1	0.0737 (4)	0.1022 (4)	0.0460 (3)	−0.0056 (3)	0.0062 (2)	−0.0110 (3)
N2	0.039 (2)	0.047 (2)	0.049 (2)	−0.0024 (16)	0.0010 (15)	0.0053 (16)
N1	0.051 (2)	0.050 (2)	0.044 (2)	0.0047 (17)	0.0001 (16)	0.0062 (17)
C7	0.032 (2)	0.042 (2)	0.045 (2)	0.0013 (19)	−0.0038 (17)	0.0074 (18)
C1	0.041 (2)	0.063 (3)	0.040 (2)	−0.008 (2)	0.0008 (18)	0.004 (2)
C11	0.051 (3)	0.052 (3)	0.046 (2)	−0.002 (2)	0.007 (2)	−0.002 (2)
C4	0.030 (2)	0.047 (2)	0.051 (2)	−0.0038 (18)	−0.0002 (18)	0.005 (2)
C12	0.070 (3)	0.060 (3)	0.041 (2)	0.002 (2)	0.007 (2)	0.013 (2)
C8	0.043 (2)	0.055 (3)	0.046 (2)	0.002 (2)	−0.0061 (19)	0.006 (2)

C3	0.046 (2)	0.045 (2)	0.058 (3)	0.008 (2)	−0.001 (2)	0.008 (2)
C6	0.051 (3)	0.049 (3)	0.062 (3)	0.003 (2)	0.004 (2)	−0.001 (2)
C13	0.067 (3)	0.057 (3)	0.044 (2)	0.009 (2)	0.005 (2)	0.008 (2)
C2	0.047 (3)	0.066 (3)	0.046 (2)	0.007 (2)	−0.0042 (19)	0.008 (2)
C5	0.044 (2)	0.051 (3)	0.048 (2)	0.006 (2)	−0.0076 (19)	0.013 (2)
C9	0.044 (2)	0.041 (2)	0.048 (2)	0.0035 (19)	0.0013 (18)	0.0050 (19)
C10	0.047 (3)	0.042 (2)	0.059 (3)	0.002 (2)	0.002 (2)	0.000 (2)

Geometric parameters (Å, º)

Br2—C11	1.880 (4)	C4—C5	1.383 (6)
Br1—C1	1.886 (4)	C12—C13	1.346 (6)
N2—C8	1.365 (5)	C12—H12	0.9300
N2—C10	1.382 (5)	C8—H8	0.9300
N2—C9	1.389 (5)	C3—C2	1.366 (6)
N1—C9	1.331 (5)	C3—H3	0.9300
N1—C7	1.369 (5)	C6—C5	1.386 (6)
C7—C8	1.364 (6)	C6—H6	0.9300
C7—C4	1.473 (6)	C13—C9	1.401 (6)
C1—C2	1.378 (6)	C13—H13	0.9300
C1—C6	1.385 (6)	C2—H2	0.9300
C11—C10	1.353 (6)	C5—H5	0.9300
C11—C12	1.407 (6)	C10—H10	0.9300
C4—C3	1.375 (6)		
C8—N2—C10	131.2 (4)	C2—C3—C4	121.4 (4)
C8—N2—C9	106.6 (3)	C2—C3—H3	119.3
C10—N2—C9	122.2 (4)	C4—C3—H3	119.3
C9—N1—C7	104.8 (3)	C1—C6—C5	118.1 (4)
C8—C7—N1	111.4 (4)	C1—C6—H6	120.9
C8—C7—C4	128.9 (4)	C5—C6—H6	120.9
N1—C7—C4	119.7 (4)	C12—C13—C9	120.1 (4)
C2—C1—C6	120.5 (4)	C12—C13—H13	119.9
C2—C1—Br1	120.6 (3)	C9—C13—H13	119.9
C6—C1—Br1	119.0 (4)	C3—C2—C1	120.0 (4)
C10—C11—C12	121.9 (4)	C3—C2—H2	120.0
C10—C11—Br2	119.9 (3)	C1—C2—H2	120.0
C12—C11—Br2	118.2 (3)	C4—C5—C6	122.0 (4)
C3—C4—C5	118.0 (4)	C4—C5—H5	119.0
C3—C4—C7	122.8 (4)	C6—C5—H5	119.0
C5—C4—C7	119.2 (4)	N1—C9—N2	111.0 (3)
C13—C12—C11	119.8 (4)	N1—C9—C13	130.6 (4)
C13—C12—H12	120.1	N2—C9—C13	118.3 (4)
C11—C12—H12	120.1	C11—C10—N2	117.6 (4)
C7—C8—N2	106.1 (4)	C11—C10—H10	121.2
C7—C8—H8	127.0	N2—C10—H10	121.2
N2—C8—H8	127.0		

C9—N1—C7—C8	0.9 (5)	C6—C1—C2—C3	2.4 (7)
C9—N1—C7—C4	−178.9 (4)	Br1—C1—C2—C3	−176.7 (3)
C8—C7—C4—C3	1.1 (6)	C3—C4—C5—C6	−1.0 (6)
N1—C7—C4—C3	−179.1 (4)	C7—C4—C5—C6	179.9 (4)
C8—C7—C4—C5	−179.8 (4)	C1—C6—C5—C4	1.2 (6)
N1—C7—C4—C5	0.0 (6)	C7—N1—C9—N2	−0.7 (4)
C10—C11—C12—C13	−0.5 (7)	C7—N1—C9—C13	178.7 (5)
Br2—C11—C12—C13	−178.9 (4)	C8—N2—C9—N1	0.3 (5)
N1—C7—C8—N2	−0.8 (5)	C10—N2—C9—N1	−178.8 (4)
C4—C7—C8—N2	179.0 (4)	C8—N2—C9—C13	−179.2 (4)
C10—N2—C8—C7	179.3 (4)	C10—N2—C9—C13	1.7 (6)
C9—N2—C8—C7	0.3 (4)	C12—C13—C9—N1	179.3 (5)
C5—C4—C3—C2	1.5 (6)	C12—C13—C9—N2	−1.4 (7)
C7—C4—C3—C2	−179.4 (4)	C12—C11—C10—N2	0.8 (6)
C2—C1—C6—C5	−1.8 (6)	Br2—C11—C10—N2	179.2 (3)
Br1—C1—C6—C5	177.3 (3)	C8—N2—C10—C11	179.8 (4)
C11—C12—C13—C9	0.8 (7)	C9—N2—C10—C11	−1.4 (6)
C4—C3—C2—C1	−2.2 (7)		

Hydrogen-bond geometry (Å, º)

*Cg*3 is the centroid of C1–C6 ring

D—H⋯*A*	*D*—H	H⋯*A*	*D*⋯*A*	*D*—H⋯*A*
C5—H5⋯N1	0.93	2.47	2.827 (5)	103
C3—H3⋯*Cg*3[i]	0.93	2.91	3.5670 (1)	129

Symmetry code: (i) *x*, −*y*−3/2, *z*−1/2.

Summary of short interatomic contacts (Å)

Contact	Distance	symmetry
H5⋯H5	2.24	*1-x,2-y,-z*
Br1⋯H12	3.01	*x,3/2-y,-1/2+z*